

Structure and allosteric regulation of the $\alpha X\beta 2$ integrin I domain

Thomas Vorup-Jensen^{*†‡}, Christian Ostermeier^{*§}, Motomu Shimaoka^{*¶}, Ulrich Hommel[§], and Timothy A. Springer^{*†¶}

^{*}Center for Blood Research, Departments of [†]Pathology and [¶]Anesthesia, Harvard Medical School, 200 Longwood Avenue, Boston, MA 02115; and [§]Protein Structure Unit, Novartis Pharma AG, Lichtstrasse 35, CH-4002 Basel, Switzerland

Contributed by Timothy A. Springer, December 4, 2002

The integrin $\alpha X\beta 2$ (CD11c/CD18, p150,95) binds ligands through the I domain of the αX subunit. Ligands include the complement factor fragment iC3b, a key component in the innate immune defense, which, together with the expression of $\alpha X\beta 2$ on dendritic cells and on other leukocytes, suggests a role in the immune response. We now report the structure of the αX I domain resolved at 1.65 Å by x-ray crystallography. To analyze structural requirements for ligand binding we made a mutation in the αX I domain C-terminal helix, which increased the affinity for iC3b ≈ 200 -fold to 2.4 μM compared with the wild-type domain affinity of ≈ 400 μM . Gel permeation chromatography supported a conformational change between the wild-type and mutated domains. Conservation of allosteric regulation in the αX I domain points to the functional importance of this phenomenon.

The integrin $\alpha X\beta 2$ (complement receptor 4, p150,95, CD11c/CD18) has an important role in host defense. $\alpha X\beta 2$ functions as a receptor for the complement C3 cleavage product iC3b (1), fibrinogen (2), denatured proteins (3), and intercellular adhesion molecule (ICAM)-1 (4). $\alpha X\beta 2$, $\alpha L\beta 2$, $\alpha M\beta 2$, and $\alpha D\beta 2$ constitute the $\beta 2$ family of integrins that are exclusively expressed on leukocytes (5). Among these, $\alpha X\beta 2$ has a unique cellular distribution with expression on monocytes and macrophages, and of particular note, on the CD8⁻ subsets of dendritic cells, which play a pivotal role in priming and regulation of the immune response (6). In the mouse, $\alpha X\beta 2$ is a marker for dendritic cells and is the predominant leukocyte integrin on these cells (7).

The ligand-binding activity of integrins is dynamically regulated by the cells on which they are expressed in a process termed “inside-out signaling” (8). The $\beta 2$ integrins are inactive in resting leukocytes and become active after cellular stimulation, as has been demonstrated for the $\alpha L\beta 2$ and $\alpha M\beta 2$ integrins. However, cellular stimulation does not affect all integrins uniformly, and $\alpha X\beta 2$ is less susceptible to activation than other $\beta 2$ integrins. Although alveolar macrophages and U937 cells coexpress $\alpha X\beta 2$ and $\alpha M\beta 2$, stronger stimulation is required to activate ligand binding by $\alpha X\beta 2$ than by $\alpha M\beta 2$ (9). Furthermore, $\alpha L\beta 2$ and $\alpha M\beta 2$ are constitutively active in 293T and COS cell transfectants, whereas $\alpha X\beta 2$ is not (10). By contrast, interspecies heterodimers containing the human αX subunit associated with either chicken or mouse $\beta 2$ subunits are active in transfectants, and this observation has been used to map $\beta 2$ residues that restrain activation of $\alpha X\beta 2$ (11) to an α - β interface in the bent conformation of integrins (12).

Ligand binding by $\alpha X\beta 2$ is mediated by the I domain of the αX subunit (13). However, the structure of the αX I domain remains undefined, despite recent advances on the structures of the αM , αL , and $\alpha 2$ I domains (14–17). I domains are members of the VWA domain family. The fold resembles that of small G proteins, with seven amphipathic helices surrounding a hydrophobic β -sheet core (15). A Mg^{2+} ion is ligated at a metal-ion-dependent adhesion site (MIDAS) at the ligand-binding “top” face of the domain, at the C-terminal ends of the parallel β -strands. At the opposite, “bottom” end of the domain, the N and C termini of the I domain connect to the β -propeller domain.

Structural studies on the I domains of the αL , αM , and $\alpha 2$ subunits suggest that transition between two conformations termed open and closed regulates ligand binding. The closed conformation is adopted in the absence of ligand binding (14–16) and is stabilized by small molecules that antagonize ligand binding (18). The open conformation is visualized when the I domain is bound to ligand (19) and also when ligand-mimetic lattice contacts are present. The open and closed conformations differ at the MIDAS, where two of the three loops that form the MIDAS shift in conformation, and the coordination of the metal is altered, making it more electrophilic for a negatively charged glutamic acid residue in the ligand that directly coordinates the metal (19, 20). This alteration is linked to a marked shift in conformation of the $\beta 6$ - $\alpha 7$ loop, and a 10-Å movement of the C-terminal, $\alpha 7$ -helix down the side of the domain. Mutations designed to stabilize the open conformation relative to the closed conformation markedly increase the affinity of the αL and αM I domains for ligand (21, 22). In one approach, Ile-316 in the $\alpha 7$ -helix of the αM I domain is mutated to Gly or removed by truncation at this position (23). Ile-316 fits into a socket formed by four hydrophobic residues in the closed conformation, but the downward movement of the $\alpha 7$ -helix in the open conformation displaces this residue to a position where it can no longer interact with the side of the I domain. In contrast to results with the αL , αM , and $\alpha 2$ I domains, recent studies with the closely related von Willebrand factor-A1 domain reveal no similar movement of the $\alpha 7$ -helix associated with ligand binding (24).

The three-dimensional structure of the αX I domain has thus far not been defined, and there is no evidence for conformational change in the αX I domain, or that conformational change regulates its ligand-binding activity. Furthermore, the affinity and kinetics of ligand binding by $\alpha X\beta 2$ or its I domain have not been measured. The finding in previous reports that $\alpha X\beta 2$ appears to be restrained in the inactive state more so than $\alpha M\beta 2$ and $\alpha L\beta 2$ (10, 11, 25) could potentially arise from differences in the allosteric control of their I domains, or of other domains that indirectly regulate ligand binding. Here, we determine the structure of the αX I domain in the closed conformation. Based on this structure, we introduce a mutation designed to destabilize the closed conformation relative to the open conformation. Affinity and kinetic measurements demonstrate a marked enhancement of binding to iC3b. Furthermore, physicochemical measurements demonstrate that the αX I domain undergoes conformational change.

Materials and Methods

Expression Constructs and Purification of Recombinant αX I Domains.

Recombinant αX I domain for x-ray crystallography was prepared by PCR amplification from cloned cDNA (kindly provided

Abbreviation: MIDAS, metal-ion-dependent adhesion site.

Data deposition: The atomic coordinates and structure factors have been deposited in the Protein Data Bank, www.rcsb.org (PDB ID code 1N3V).

[†]T.V.-J. and C.O. contributed equally to this work.

[¶]To whom correspondence should be addressed. E-mail: springeroffice@cbr.med.harvard.edu.

by Marion Mahnke, Novartis Pharma) contained in pET15b vector (Novagen) of a sequence encoding residues Ser-122 to Gly-319. “Sticky-end PCR” (26) was carried out with PfuTurbo (catalog no. 600250, Stratagene) with either the sense primer 5'-TATGGCTAGCAGACAGGAGCAGGAC-3' or 5'-TG-GCTAGCAGACAGGAGCAGGAC-3' (the portion of the restriction sites contained in the primer sequences are underlined and protein coding sequences are capitalized), which mutated Cys-126 to glutamine, and with the T7 terminator primer (catalog no. 69337-3, Novagen) as antisense primer. The two PCR products were combined, heated to 95°C, and cooled on ice. After digestion with *Bam*HI, the fragment was cloned into the *Nde*I and *Bam*HI sites of the pET28a vector (Novagen). The plasmid was transformed into *Escherichia coli* BL21(DE3) (Novagen). The transformed bacteria were cultivated in LB with kanamycin selection. Recombinant protein synthesis was induced when the bacterial culture reached an optical density at 650 nm of 0.5–1.0 by addition of isopropyl β -D-thiogalactopyranoside (IPTG) to a final concentration of 1 mM. After 3 h of cultivation at 25°C, bacteria from 4 liters of culture were harvested by centrifugation. Frozen cells were resuspended in 5 vol of 300 mM NaCl/10% (vol/vol) glycerol/1 mM PMSF/5 mM MgCl₂/0.1% (vol/vol) 2-mercaptoethanol/1 mg of lysozyme per ml/0.5% (vol/vol) *t*-octylphenoxypolyethoxyethanol (Triton X-100)/50 mM NaH₂PO₄, pH 8.0, followed by ultrasonication. The lysate was cleared by centrifugation at 15,000 \times g for 20 min and filtration through polysulfone membranes with 0.45- μ m pores, and incubated with Ni-NTA resin (Ni-NTA Superflow, catalog no. 30410, Qiagen, Valencia, CA; 12 ml of resin per 90 ml of lysate; NTA, nitrilotriacetate). The resin was washed with 300 mM NaCl/5 mM MgCl₂/10 mM imidazole/0.1% (vol/vol) Triton X-100/50 mM NaH₂PO₄, pH 8.0. After a brief wash in the same buffer without Triton X-100, the protein was eluted in 5 mM MgCl₂/200 mM imidazole/50 mM NaH₂PO₄, pH 8.0. The protein was dialyzed for \approx 16 h against 100 mM NaCl/5 mM MgCl₂/50 mM NaH₂PO₄, pH 8.0, in the presence of 200 units thrombin per 4 liters of bacterial culture, followed by a second dialysis step against 5 mM MgCl₂/50 mM NaH₂PO₄, pH 6.0. Ion-exchange chromatography of 30 ml of lysate at \approx 1 mg/ml was carried out on a 6-ml Resource S column (catalog no. 17-1180-01, Amersham Biosciences, Uppsala), eluting the protein in a 0–750 mM NaCl gradient in 5 mM MgCl₂/25 mM NaH₂PO₄, pH 6.5. Recombinant protein-containing fractions were further purified by gel permeation chromatography on a 1 \times 30 cm Superdex 75-HR column (catalog no. 17-1047-01, Amersham Biosciences) in 20 mM NaH₂PO₄/5 mM MgCl₂, pH 7.0.

For functional analysis of α X I domains of wild-type or mutant sequence, the sequence coding for the residues Val-121 to Gly-319 was amplified from cloned cDNA (27) as template by PCR (Expand High Fidelity PCR, catalog no. 1-732-641, Roche Diagnostics, Rotkreuz, Switzerland) with the sense primer 5'-tagtagattAATGGTGTCCAGGCAGGAGTCCCA-3' containing an *Ase*I restriction endonuclease site and the start codon as well as mutating Cys-126 to serine. Amplification of the wild-type α X I domain sequence was carried out with the antisense primer 5'-ctactagtcgactcatcagtGATGGTGATGGTGATGACCCTCAATGGCAAAGATCTTCTCC-3' containing a His₆ tag followed by the stop codon and a *Sal*I restriction site, whereas the Ile-314 \rightarrow Gly-encoding construct was made with the antisense primer 5'-catctagtcgactcatcagtGATGGTGATGGTGATGACCCTCAATGGCAAAGCCCTTC-TCCTT-3'. The PCR products were cloned into the *Nde*I and *Sal*I sites of the pET20b(+) vector (Novagen) by using transformation-competent *E. coli* DH5 α (18258–012; GIBCO/BRL) followed by subcloning into *E. coli* BL21(DE3).

A clone of the BL21 transformants was inoculated into 200 ml of LB with 100 μ g of ampicillin per ml (LB/amp) and cultured

at 37°C for 16 h. The culture was diluted 10-fold in LB/amp. After culturing for 1 h, expression was induced by adding isopropyl β -D-thiogalactopyranoside to a final concentration of 1 mM. Lysis and purification on Ni-NTA beads was carried out essentially as described above. Typically, the preparation of the recombinant protein was >90% pure as estimated by SDS/PAGE and Coomassie brilliant blue staining, with a yield of \approx 3 mg per liter of bacterial culture. Small aggregates were removed by centrifugation and filtration of the sample through a polysulfone membrane filter with 0.22- μ m pores, and the protein was further purified by subjecting 2 ml of the preparation to gel permeation chromatography on a HiLoad 1.6 \times 60 cm Superdex 75 preparatory grade column (catalog no. 17-1068-01, Amersham Pharmacia) in 10 mM of [2-(*N*-morpholino)ethanesulfonic acid](Mes)/100 mM NaCl, pH 5.0, at 1 ml/min. The recombinant protein eluted in a single, sharp peak at $V_e = 75.0$ ml for the wild-type protein and at $V_e = 74.1$ ml for the Ile-314 \rightarrow Gly mutant. No contaminating proteins could be observed in the recombinant protein-containing fractions as analyzed by Coomassie brilliant blue-stained SDS/PAGE gels.

Crystallization, Data Collection, Determination of the Structure, and Structural Analysis. Crystals were grown from solutions containing 20 mg/ml α X I domain (Ser-122 through Gly-319) in 20 mM Hepes, pH 7.0. An initial screen was performed by using JBScreen 6 ammonium sulfate-based buffers (JenaBioSciences, Jena, Germany). Optimization of the conditions suggested that the glycerol concentration was a critical factor. A grid screen varying ammonium sulfate versus glycerol concentrations showed that crystals could be grown at ammonium sulfate concentrations of 2.2–2.6 M in the presence of 17.5% or 20% (vol/vol) glycerol/100 mM sodium acetate, pH 5.0, with 5 mM EDTA or 15 mM MnCl₂. A crystal was mounted into a capillary and diffraction data were collected at room temperature with a rotation anode generator equipped with a copper target. One hundred images were collected with 1.0° oscillation each. Raw diffraction data were processed and scaled with the HKL program suite Version 1.96.6 (28).

Theoretical calculations on the hydrodynamic properties of the recombinant proteins from their predicted three-dimensional structures were carried out as described by Carrasco and Garcia de la Torre (29) using the program HYDRO version 3c (<http://leonardo.fcu.um.es/macromol>). For hydrodynamic calculations, residues that were disordered in the α X structure (Val-121 through Arg-128, and Glu-318, Gly-319, and the His₆ tag) were modeled using SEGMOD (30). To model the open conformation of the α X I domain Ile-314 mutant, the open α M structure 1IDO (20) was used as template. The model of residues Val-121 through Arg-128, and the C-terminal residues including the His₆ tag from the closed conformation model were included as templates for the open α X model, so that the unresolved regions of both conformations were very similar, and should not introduce bias into the hydrodynamic calculations.

Molecular Size Estimation Under Nondenaturing and Denaturing Conditions. Peak fractions from the gel permeation chromatography purification were collected and rechromatographed on a 1 \times 30 cm Superdex 75-HR column connected to the ÄKTA FPLC system (Amersham Pharmacia) in 150 mM NaCl/0.05% (vol/vol) Tween-20/10 mM Hepes, pH 7.4 (HBS/Tw), with 1 mM EDTA and with a flow rate of 1 ml/min. Before gel permeation chromatography, the samples of recombinant I domains were mixed with blue dextran 2000 and bovine aprotinin (catalog no. A-6279, Sigma) and adjusted to a total sample volume of 100 μ l with HBS/Tw. A standard curve for estimation of Stokes radius (R_s) was established by comparison with the elution volumes of

ribonuclease A, chymotrypsinogen, ovalbumin, BSA, and blue dextran 2000 (catalog no. 17-0442-01, low molecular weight gel filtration calibration kit, Amersham Pharmacia).

Molecular size estimation under denaturing conditions was carried out by SDS/PAGE on 4–20% Tris-glycine gradient gels (PAGEr precast gels, catalog no. 58511, BioWhittaker). The samples of recombinant I domains were boiled briefly in sample buffer, electrophoresed, and Coomassie brilliant blue R-250 (catalog no. 61-0400, Bio-Rad) stained (31). Protein standards were Precision Protein Standard (catalog no. 161-0362, Bio-Rad).

Surface Plasmon Resonance Assays. Preparation of B1 Pioneer sensor chips (catalog no. 99-1000-02, Biacore, Uppsala) and recording of sensorgrams was carried out on the BIAcore 1000 instrument. Activation of surfaces, immobilization of proteins through primary amine coupling, and blocking of unreacted sites in the flow cells was carried out according to the kit manufacturer's instructions (Amine coupling kit, catalog no. BR-1000-50, Biacore). Ligand interaction was tested on surfaces with 4,900–5,000 response units (RUs) of immobilized iC3b (catalog no. 204863, Calbiochem) or a surface activated as above and blocked with ethanolamine.

Interaction with the iC3b-coated- or control surface was tested in running buffer containing 150 mM NaCl, 10 mM Mes, pH 6.0, with 1 mM MgCl₂ (Mes/Mg) or 1 mM EDTA as appropriate. The I domain preparations were diluted in Mes/Mg and injected at the indicated concentrations. Surfaces were regenerated in 1.5 M NaCl/100 mM Hepes, pH 7.4, with 20 mM EDTA. Kinetic analysis was carried out by use of the BIAEVALUATION 3.0 software (Biacore) after subtracting the response on the control surface from the signal obtained on the iC3b-coated surface. K_d was calculated by steady-state analysis and k_{off} was derived from local curve fitting on the dissociation phases. k_{on} was calculated from the K_d and k_{off} . The binding was also analyzed by global fitting of the sensorgram data to Langmuir adsorption isotherms.

Results

Structure of α X I Domain at 1.65 Å. A recombinant protein with residues Ser-122 through Gly-319 of the α X I domain was crystallized in 2.2 M ammonium sulfate/20% glycerol/5 mM EDTA or 2.6 M ammonium sulfate/17.5% glycerol/15 mM MnCl₂/100 mM sodium acetate, pH 5.0. Both structures were solved by molecular replacement using CNX (32) and a 1.35-Å resolution structure of the human α M I domain (data not shown) as a search model. The two crystallization conditions yielded identical crystal forms, and in each case the structures lacked a metal at the MIDAS. The crystals in MnCl₂ gave the best diffraction data, with a resolution of 1.65 Å. The initial R factor after a cycle of rigid body refinement was 0.334 ($R_{free} = 0.346$). The α X I domain model was built with o (33) and refined with CNX 2000 to an R factor of 20.8% and R_{free} of 22.5% (Table 1).

The α X I domain adopts a G protein-like α/β Rossmann fold characterized by alternating amphipathic α -helices and hydrophobic β -strands (Figs. 1A and 2B). Five parallel β -strands form a central hydrophobic sheet together with a sixth antiparallel strand (β 3). The central β -sheet is surrounded by seven α -helices. The α X I domain clearly adopts the closed conformation; it superimposes on the closed α M I domain structure (15) with an rms deviation of 0.99 Å (Fig. 1A), but on the open α M I domain structure with an rms deviation of 2.9 Å, for all C α atoms from Glu-130 through Lys-313 (α X numbering). No metal ion is bound at the MIDAS; however, the side chains of MIDAS residues are oriented similarly to those in I domain structures in the closed conformation (Fig. 1B). There is a close lattice contact with the C-terminal part of the α 5-helix at the MIDAS, and a water molecule or ammonium ion forms a hydrogen bond network with the side chains of MIDAS residues Asp-138,

Table 1. Crystallography data and refinement statistics

Crystallography data	
No. of crystals	1
Space group	$P6_1$
Unit cell dimensions	
$a, b, c, \text{Å}$	84.7, 84.7, 65.8
$\alpha, \beta, \gamma, ^\circ$	90, 90, 120
No. of monomers per atomic unit	1
Solvent content, %	61
Resolution range, Å	30–1.65
No. of reflections	
Observed	278,307
Unique	32,389
Overall	
Data redundancy	5.4
Data completeness, %	99.9
$\langle I/\sigma(I) \rangle$	14.9
R_{merge}	0.061
Highest-resolution shell	
Resolution range, Å	1.71–1.65
Completeness for shell, %	100.0
R_{merge} for shell	0.229
Reflections with $I \geq 3\sigma(I)$, %	55.8
Refinement statistics	
Data used in refinement	
Resolution range, Å	27.72–1.65
Intensity cutoff [$\Sigma(F)$]	0.0
No. of reflections	32,311
Completeness (working + test set), %	99.8
Fit to data used in refinement	
Overall R_{crist}	0.208
Overall R_{free}	0.225
No. of nonhydrogen atoms	
Protein atoms	1,513
Waters	292
rms deviations from ideal values	
Bond lengths, Å	0.005
Bond angles, °	1.2
Dihedral angles, °	23.2
Improper angles, °	0.72

Thr-207, and Asp-240. The water molecule or ammonium ion can be distinguished from a metal by its B factor, the longer distances observed for hydrogen bonds than metal–ligand bonds, and its distinct position in the MIDAS (Fig. 1B). The presence or absence of a metal ion at the MIDAS has previously been shown to have little effect on its conformation (15, 16, 34, 35).

In the ligand-binding region around the MIDAS, there are substantial differences between the α X and α M I domains (Fig. 1C), which are reflected in differences in the electrostatic surfaces (Fig. 1E and F). There are two substitutions of charged residues in α M (Arg-208 and Asp-273) for hydrophobic residues in α X (Phe-206 and Leu-271). Furthermore, Glu-244 and Phe-246 in α M are replaced by Lys-242 and Glu-244 in α X, respectively. These differences have important implications for the ligand-binding specificities of α X β 2 and α M β 2.

Comparison of the β 6- α 7 segment to other closed I domain structures (Fig. 2A) confirms that the α X I domain is in the closed conformation. In the α X I domain structure, the C-terminal α 7-helix is tightly associated with the body of the domain through hydrophobic residue contacts (Fig. 2A). In the α M and α 2 I domains, this α -helix also packs well; however, in the α L I domain, multiple structures show that the α 7-helix is flexible, and often does not pack against the side of the domain (Fig. 2A) Near the end of the α 7-helix, the side chain of Ile-314

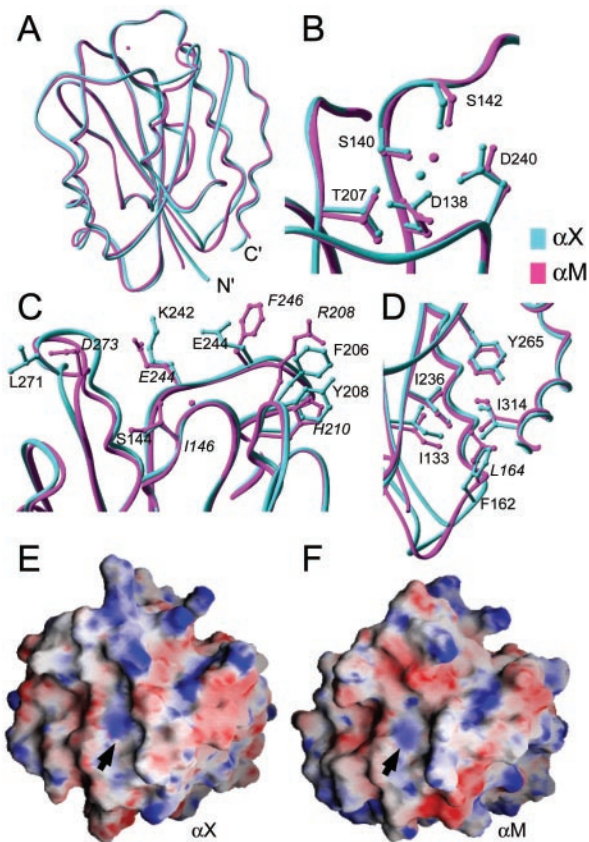


Fig. 1. The αX I domain structure and comparison to the αM I domain. (A–D) Comparison of αX (cyan) and the αM (magenta) I domains. The MIDAS metal ion present only in αM is shown as a magenta sphere, and the water molecule oxygen present only in the αX MIDAS is shown as a cyan sphere. (A) Backbones of αX and αM . (B) MIDAS region of the αX and αM I domains. Residue numbers refer to the αX sequence. (C) Residues in proximity of the αX and αM MIDAS, which form part of a putative ligand-binding interface and differ in structure or polarity between the two I domains (αX and αM residues are labeled in roman and italics, respectively). (D) Detail of the region forming the hydrophobic socket for Ile-314 (αX) or Ile-316 (αM). Residue numbers refer to the αX sequence, and Leu-164 of αM is labeled in italics. All figures were made with RIBBONS software (41). (E and F) Electrostatic surfaces of the αM and αX I domains. The molecular surfaces of the domains were constructed with GRASP (42). The electrostatic potentials were calculated with the Delphi algorithm (43) and mapped onto the molecular surfaces on a scale from -10 kT/e $^-$ (red) to $+10$ kT/e $^-$ (blue). A Mg $^{2+}$ ion was placed at the αX I domain MIDAS to make the electrostatic surfaces comparable. Positions of the metal ions in the αX and αM I domains are indicated with arrows.

of the αX I domain is buried in a hydrophobic socket formed by the side chains of Ile-133, Phe-162, Ile-234, and Tyr-265 (Fig. 1D). The highly conserved Ile in this position is buried in a similar socket in the αM (Fig. 1D) and $\alpha 2$ I domains, but not in the αL I domain (Fig. 2A; ref. 23). The residues forming the socket are conserved between αX and αM , except Phe-162 in αX replaces a Leu in αM (Fig. 1D).

Activation of iC3b Ligand Binding by Mutation of Ile-314 to Gly. To destabilize the closed conformation of the αX I domain relative to the open conformation, Ile-314 was mutated to glycine to disrupt the contact between this residue and the hydrophobic socket. Binding measured by surface plasmon-resonance chip surfaces coated with the αX antibody 3.9 (36) (data not shown) confirmed the structural integrity of both the mutant and wild-type I domains. Ligand binding by the wild-type and Ile-314 \rightarrow Gly-mutated αX I domains was tested by surface plasmon resonance on chip surfaces coated with iC3b. In the presence of Mg $^{2+}$ the Ile-314 \rightarrow Gly mutant bound strongly to iC3b (Fig. 3A). The wild-type domain bound iC3b too weakly to accurately measure kinetics or K_d values. No binding was detectable in the concentration range used for measurement of binding of the Ile-314 \rightarrow Gly mutant. However, binding was detected at 25.6 μM wild-type I domain (Fig. 3B) that was comparable to the amount of binding obtained with 0.138 μM mutant I domain (Fig. 3A). Therefore, the K_d differs by approximately the ratio of these two concentrations, i.e., ≈ 200 -fold. Binding was highly specific, because in EDTA it was undetectable at the highest protein concentrations tested, 12.8 and 25.6 μM for the mutant and wild-type I domains, respectively (Fig. 3C). No significant binding of the Ile-314 \rightarrow Gly mutant was observed when 1 mM Ca $^{2+}$ was substituted for Mg $^{2+}$. Two different methods used to estimate k_{on} , k_{off} , and K_d for binding of the Ile-314 \rightarrow Gly mutant to iC3b in Mg $^{2+}$ gave excellent agreement (Table 2). The K_d for the Ile-314 \rightarrow Gly mutant was close to 2.2 μM with average k_{on} and k_{off} values of 8,400 M $^{-1}$ s $^{-1}$ and 0.0215 s $^{-1}$, respectively.

Physicochemical Properties of Wild-Type and Ile-314 \rightarrow Gly Mutant αX I Domains. The mutant and wild-type αX I domains were purified by gel permeation chromatography before surface plasmon resonance measurements. Both proteins eluted as monomeric, symmetric peaks; however, their elution volumes differed significantly. To quantify and confirm these differences, samples of purified material were rechromatographed on an analytical Superdex 75 column in 150 mM NaCl/10 mM Hepes, pH 7.4 buffer containing 1 mM EDTA to ensure that

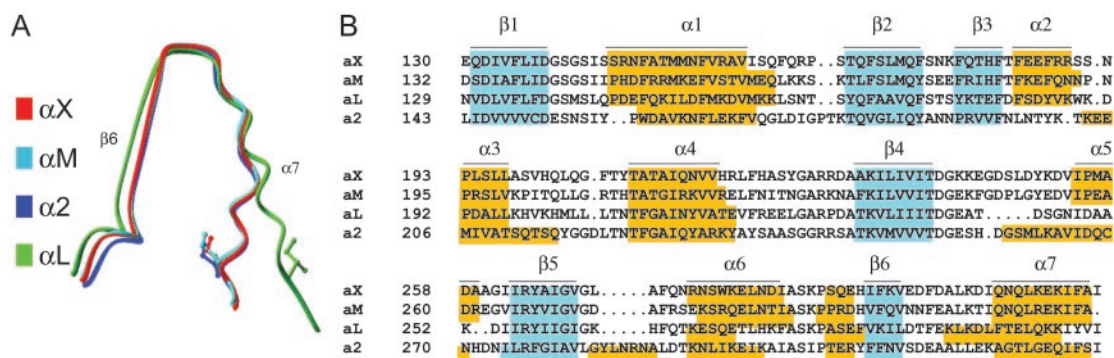


Fig. 2. Comparisons among closed I domain structures of the C-terminal $\beta 6$ -strand and $\alpha 7$ -helix. Superposition is based on the entire domain. The backbone segments shown are αX , residues 288–317; αM , residues 290–318 of 1JLM (15); $\alpha 2$, residues 306–334 of 1AOX (14); and αL , residues 280–308 of 1LFA (16). The side chains of Ile-332 in $\alpha 2$, Ile-316 in αM , Ile-314 in αX , and Ile-306 in αL are shown. (B) Structure-based sequence alignment of the αX , αM , αL , and $\alpha 2$ I domains. The same closed structures as above were superimposed. α -Helices are shown in gold and β -strands are shown in cyan. Secondary structure assignment was by the DSSP algorithm (44) from the structural coordinates.

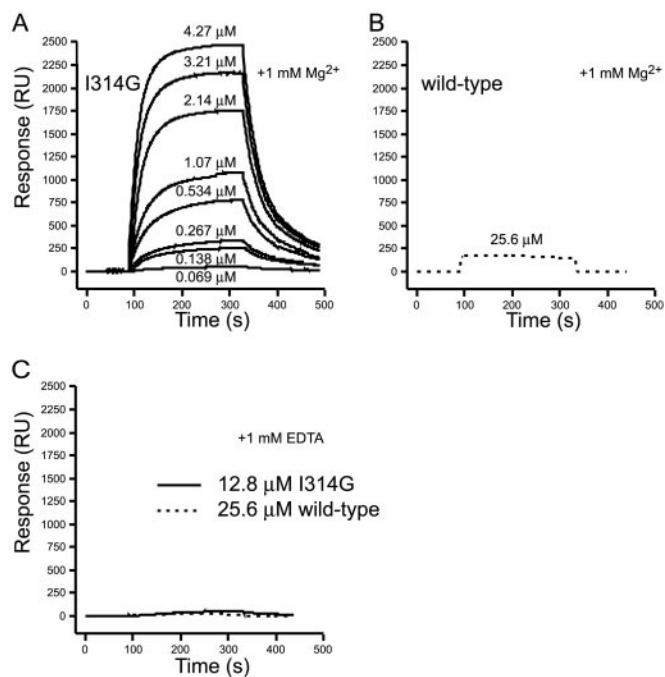


Fig. 3. Binding of the α X I domain to iC3b measured in real time with surface plasmon resonance. (A) Overlay of representative sensorgrams recording the binding of the indicated concentration of the Ile-314 \rightarrow Gly (I314G) α X domain to iC3b in the presence of 1 mM Mg^{2+} . (B) Representative sensorgram showing the binding of the wild-type α X domain at 25.6 μ M in the presence of Mg^{2+} to iC3b. (C) Binding of the wild-type (25.6 μ M) and Ile-314 \rightarrow Gly (12.8 μ M) domains in the presence of 1 mM EDTA. In all sensorgrams, the signal from the control surface was subtracted from the signal obtained on the iC3b-coated surface.

ligand-like interactions through the MIDAS did not contribute to the mobility. Similar results were obtained in 100 mM NaCl/10 mM sodium acetate, pH 5.0 (not shown). The samples were spiked with high-molecular weight blue dextran and bovine aprotinin markers to validate the reproducibility of chromatographic runs. The Ile-314 \rightarrow Gly mutant consistently eluted earlier than the wild-type α X I domain (13.27 and 13.66 ml, respectively, Fig. 4A). The hydrodynamic Stokes radii were 19.7 \AA and 17.8 \AA for the mutated and wild-type domains, respectively.

In contrast to the results under native conditions, the mutant and wild-type I domains had identical mobilities under denaturing conditions in SDS/PAGE (Fig. 4B). The M_r in SDS/PAGE of 22×10^3 closely matched the calculated M_r of 23.4×10^3 .

Discussion

We describe the crystal structure of the I domain of the integrin α X subunit, and demonstrate that the conformation of the α X

Table 2. Kinetics of Ile-314 \rightarrow Gly mutant α X I domain binding to iC3b

Analysis	k_{on} , $M^{-1}s^{-1}$	k_{off} , s^{-1}	K_d , μ M
Steady state*	$9,200 \pm 3,300$	0.0220 ± 0.003	2.38 ± 0.71
Langmuir binding†	$7,650 \pm 920$	0.0158 ± 0.002	2.09 ± 0.40

Values are the mean \pm SD from three experiments.

* k_{off} was determined by curve-fitting to the postinjection part of the sensorgrams. K_d was determined from the steady-state equilibrium response levels and k_{on} was calculated as k_{off}/K_d .

† k_{on} and k_{off} were determined by curve-fitting to Langmuir adsorption isotherms and K_d was calculated as k_{off}/k_{on} .

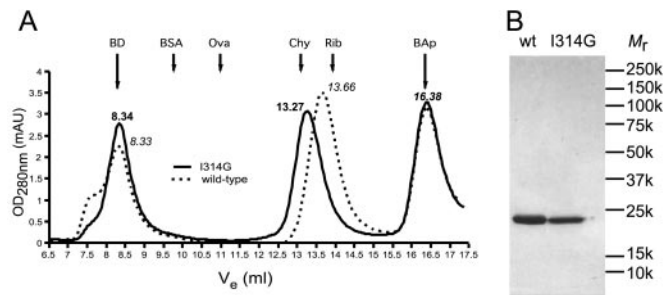


Fig. 4. Molecular size estimation under nonreducing and denaturing conditions. (A) Representative elution profiles from analytical gel permeation chromatography of either the wild-type (dotted line, peak elution volumes are indicated in italics) or the Ile-314 \rightarrow Gly mutant (solid line, peak elution volumes are indicated in bold) α X I domains. The samples were spiked with blue dextran (BD) eluting at the excluded volume of the column (8.34 ml) and bovine aprotinin (BAp), which eluted at 16.38 ml (the peak elution volumes of both internal markers are indicated with long arrows). The bed volume of the column was 18 ml. The column was calibrated with bovine serum albumin (BSA; 67.0 kDa, $R_s = 35.5 \text{\AA}$), ovalbumin (Ova; 43.0 kDa, $R_s = 30.5 \text{\AA}$), chymotrypsinogen A (Chy; 25.0 kDa, $R_s = 20.9 \text{\AA}$), and ribonuclease A (Rib; 13.7 kDa, $R_s = 16.4 \text{\AA}$). The peak elution volumes of the size markers are indicated with short arrows. (B) Nonreducing SDS/PAGE of the wild-type (wt) and Ile-314 \rightarrow Gly mutant α X I domain.

I domain modulates its affinity for ligand. It has previously been demonstrated that cellular stimulation can activate ligand binding by the α X β 2 integrin on the cell surface; however, there has been no evidence that the conformation of the α X I domain regulates ligand binding. Comparison to other I domain structures shows that the 1.65- \AA resolution structure determined here for the α X I domain is in the closed conformation.

Previously, mutations that stabilize the open conformation relative to the closed conformation, or that destabilize the closed conformation relative to the open conformation, have been shown to markedly increase ligand binding by the α L and α M I domains (21, 23, 37). Several studies have targeted the C-terminal α 7-helix and the loop preceding this helix, and have shown that although distal from the ligand-binding site at the MIDAS, the conformation of the β 6- α 7 loop is tightly allosterically linked to ligand-binding affinity. In α M, the mutation of Ile-316 to glycine, or truncation at residue 315 in the C-terminal helix, activates ligand binding (23). This Ile packs in a “socket for isoleucine” in the closed conformation; whereas when the α -helix moves 10 \AA down the side of the domain in the open conformation, Ile-316 is displaced to a position below the bottom of the domain and is not resolved in crystal structures. In the α X I domain, the equivalent residue is Ile-314, which fits into a hydrophobic socket very similar to that in α M, with the exception that the residue equivalent to Leu-164 in α M is Phe-162 in α X. Curiously, the Leu-164 \rightarrow Phe mutation in the α M β 2 holoreceptor increased ligand-binding activity, presumably by destabilizing the packing against the domain of the α 7-helix by reducing the space available in the socket for Ile-316 (38). In α X, the backbone of the loop following the α 1-helix shifts $\approx 2 \text{\AA}$ down at the position of Phe-162 to accommodate its bulky side chain.

The packing of Ile-314 in the hydrophobic socket in the closed conformation of the α X I domain provided the structural rationale for mutating this residue to Gly to destabilize the closed conformation and shift the conformational equilibrium toward the open conformation. The mutated α X I domain bound iC3b in a Mg-dependent manner with a K_d of 2.2 μ M. This affinity was increased ≈ 200 -fold relative to the wild-type I domain in the closed conformation. Therefore, the affinity of the α X I domain for ligand is dramatically regulated through con-

formational change, providing an explanation for the biological regulation of ligand binding by the $\alpha X\beta 2$ holoreceptor.

We directly confirmed a conformational change in solution by an increase in the hydrodynamic Stokes radius of the mutant αX I domain. An increase in radius was expected because the downward shift of the C-terminal helix to a position beyond the base of the I domain would make it more extended. Modeling the open αX I domain conformation and computation of Stokes radii from the structural coordinates (see *Materials and Methods* and refs. 29 and 39) predicts an increase of 0.6 Å in Stokes radius for the open conformation. The larger observed increase of 2 Å compared with the predicted increase of 0.6 Å may reflect an extended conformation of the portion of the $\alpha 7$ -helix that extends below the bottom of the domain in the open conformation, whereas we modeled it as helical. The hydrodynamic measurements directly demonstrate conformational change. Furthermore, the elution peaks for the wild-type and mutant I domains were equally sharp. This finding shows that the mutant I domain does not exist as a stable mixture of open and closed conformers. The mutant αX I domain, thus, is either stable in the open conformation or is in rapid equilibration between the open and closed structures.

Although the overall structures of the αM and αX I domains are similar, multiple residues in proximity of the MIDAS differ between the αM and αX I domains, with fewer charged residues in the αX I domain. The $\alpha X\beta 2$ and $\alpha M\beta 2$ integrins recognize an overlapping set of ligands with no structural homology, including iC3b, ICAM-1, and fibrinogen. A binding site in fibrinogen for both I domains has been mapped to the C-terminal region of the fibrinogen γ chain (40). Given this similarity, it is surprising that the ligand-binding surfaces surrounding the MIDAS of the αX and αM I domains are so varied. By contrast, $\alpha L\beta 2$ recognizes structurally homologous ligands, the ICAMs; furthermore, the site on ICAM-1 recognized by $\alpha L\beta 2$ differs from that recognized by $\alpha M\beta 2$ and presumably $\alpha X\beta 2$. No biological ligands have yet been crystallized with the αM or αX I domains, and our study points to important questions that remain to be answered about ligand recognition by $\alpha M\beta 2$ and $\alpha X\beta 2$.

We thank Drs. Junichi Takagi, Tsan Xiao, and Christopher Carman for helpful discussions, Moonsoo Jin for Delphi calculations, and T. Stehle for reviewing the manuscript. This work was supported by National Institutes of Health Grant CA31799 (to T.A.S.). T.V.-J. was in receipt of a fellowship (990760/20-1328 and 0122/20) from the Carlsberg Foundation, Copenhagen.

- Micklem, K. J. & Sim, R. B. (1985) *Biochem. J.* **231**, 233–236.
- Loike, J. D., Sodeik, B., Cao, L., Leucona, S., Weitz, J. I., Detmers, P. A., Wright, S. D. & Silverstein, S. C. (1991) *Proc. Natl. Acad. Sci. USA* **88**, 1044–1048.
- Davis, G. E. (1992) *Exp. Cell Res.* **200**, 242–252.
- Diamond, M. S., Garcia-Aguilar, J., Bickford, J. K., Corbi, A. L. & Springer, T. A. (1993) *J. Cell Biol.* **120**, 1031–1043.
- Gahmberg, C. G., Tolvanen, M. & Kotovuori, P. (1997) *Eur. J. Biochem.* **245**, 215–232.
- Shortman, K. & Liu, Y. J. (2002) *Nat. Rev. Immunol.* **2**, 151–161.
- Metlay, J. P., Witmer-Pack, M. D., Agger, R., Crowley, M. T., Lawless, D. & Steinman, R. M. (1990) *J. Exp. Med.* **171**, 1753–1771.
- Shimaoka, M., Takagi, J. & Springer, T. A. (2002) *Annu. Rev. Biophys. Biomol. Struct.* **31**, 485–516.
- Ross, G. D., Reed, W., Dalzell, J. G., Becker, S. E. & Hogg, N. (1992) *J. Leukocyte Biol.* **51**, 109–117.
- Bilsland, C. A. G., Diamond, M. S. & Springer, T. A. (1994) *J. Immunol.* **152**, 4582–4589.
- Zang, Q. & Springer, T. A. (2001) *J. Biol. Chem.* **276**, 6922–6929.
- Beglova, N., Blacklow, S. C., Takagi, J. & Springer, T. A. (2002) *Nat. Struct. Biol.* **9**, 282–287.
- Springer, T. A. (1997) *Proc. Natl. Acad. Sci. USA* **94**, 65–72.
- Emsley, J., King, S. L., Bergelson, J. M. & Liddington, R. C. (1997) *J. Biol. Chem.* **272**, 28512–28517.
- Lee, J.-O., Rieu, P., Arnaout, M. A. & Liddington, R. (1995) *Cell* **80**, 631–638.
- Qu, A. & Leahy, D. J. (1995) *Proc. Natl. Acad. Sci. USA* **92**, 10277–10281.
- Legge, G. B., Kriwacki, R. W., Chung, J., Hommel, U., Ramage, P., Case, D. A., Dyson, H. J. & Wright, P. E. (2000) *J. Mol. Biol.* **295**, 1251–1264.
- Weitz-Schmidt, G., Welzenbach, K., Brinkmann, V., Kamata, T., Kallen, J., Bruns, C., Cottens, S., Takada, Y. & Hommel, U. (2001) *Nat. Med.* **7**, 687–692.
- Emsley, J., Knight, C. G., Farnedale, R. W., Barnes, M. J. & Liddington, R. C. (2000) *Cell* **101**, 47–56.
- Lee, J.-O., Bankston, L. A., Arnaout, M. A. & Liddington, R. C. (1995) *Structure (London)* **3**, 1333–1340.
- Shimaoka, M., Shifman, J. M., Jing, H., Takagi, J., Mayo, S. L. & Springer, T. A. (2000) *Nat. Struct. Biol.* **7**, 674–678.
- Shimaoka, M., Lu, C., Palframan, R., von Andrian, U. H., Takagi, J. & Springer, T. A. (2001) *Proc. Natl. Acad. Sci. USA* **98**, 6009–6014.
- Xiong, J.-P., Li, R., Essafi, M., Stehle, T. & Arnaout, M. A. (2000) *J. Biol. Chem.* **275**, 38762–38767.
- Huizinga, E. G., Tsuji, S., Romijn, R. A., Schiphorst, M. E., de Groot, P. G., Sixma, J. J. & Gros, P. (2002) *Science* **297**, 1176–1179.
- Springer, T. A., Miller, L. J. & Anderson, D. C. (1986) *J. Immunol.* **136**, 240–245.
- Zeng, G. (1998) *BioTechniques* **25**, 206–208.
- Corbi, A. L., Miller, L. J., O'Connor, K., Larson, R. S. & Springer, T. A. (1987) *EMBO J.* **6**, 4023–4028.
- Otwinowski, Z. & Minor, W. (1997) *Methods Enzymol.* **276**, 307–326.
- Carrasco, B. & Garcia de la Torre, J. (1999) *Biophys. J.* **76**, 3044–3057.
- Levitt, M. (1992) *J. Mol. Biol.* **226**, 507–533.
- Sambrook, J. & Russell, D. W. (2000) *Molecular Cloning: A Laboratory Manual* (Cold Spring Harbor Lab. Press, Plainview, NY).
- Brunger, A. T., Adams, P. D., Clore, G. M., DeLano, W. L., Gros, P., Grosse-Kunstleve, R. W., Jiang, J.-S., Kuszewski, J., Nilges, M., Pannu, N. S., et al. (1998) *Acta Crystallogr. D* **54**, 905–921.
- Jones, T. A., Zou, J. Y., Cowan, S. W. & Kjeldgaard, M. (1991) *Acta Crystallogr. A* **47**, 110–119.
- Baldwin, E. T., Sarver, R. W., Bryant, G. L., Jr., Curry, K. A., Fairbanks, M. B., Finzel, B. C., Garlick, R. L., Heinrikson, R. L., Horton, N. C., Kelley, L. L., et al. (1998) *Structure (London)* **6**, 923–935.
- Qu, A. & Leahy, D. J. (1996) *Structure (London)* **4**, 931–942.
- Hogg, N., Takacs, L., Palmer, D. G., Selvendran, Y. & Allen, C. (1986) *Eur. J. Immunol.* **16**, 240–248.
- Lu, C., Shimaoka, M., Ferzly, M., Oxvig, C., Takagi, J. & Springer, T. A. (2001) *Proc. Natl. Acad. Sci. USA* **98**, 2387–2392.
- Oxvig, C., Lu, C. & Springer, T. A. (1999) *Proc. Natl. Acad. Sci. USA* **96**, 2215–2220.
- Garcia de la Torre, J., Huertas, M. L. & Carrasco, B. (2000) *Biophys. J.* **78**, 719–730.
- Ugarova, T. P. & Yakubenko, V. P. (2001) *Ann. N.Y. Acad. Sci.* **936**, 365–385.
- Carson, M. (1997) *Methods Enzymol.* **277**, 493–505.
- Nicholls, A., Sharp, K. A. & Honig, B. (1991) *Proteins* **11**, 281–296.
- Nicholls, A. & Honig, B. (1991) *J. Comput. Chem.* **12**, 435–445.
- Kabsch, W. & Sander, C. (1983) *Biopolymers* **22**, 2577–2637.